

A 3D total magnetization inversion applicable when significant, complicated remanence is present

Peter G. Lelièvre¹ and Douglas W. Oldenburg¹

ABSTRACT

Inversion of magnetic data is complicated by the presence of remanent magnetization. To deal with this problem, we invert magnetic data for a three-component subsurface magnetization vector, as opposed to magnetic susceptibility (a scalar). The magnetization vector can be cast in a Cartesian or spherical framework. In the Cartesian formulation, the total magnetization is split into one component parallel and two components perpendicular to the earth's field. In the spherical formulation, we invert for magnetization amplitude and the dip and azimuth of the magnetization direction. Our inversion schemes contain flexibility to obtain different types of magnetization models and allow for inclusion of geologic information regarding remanence. Allowing a vector magnetization increases the nonuniqueness of the magnetic inverse problem greatly, but additional information (e.g., knowledge of physical properties or geology) incorporated as constraints can improve the results dramatically. Commonly available information results in complicated nonlinear constraints in the Cartesian formulation. However, moving to a spherical formulation results in simple bound constraints at the expense of a now nonlinear objective function. We test our methods using synthetic and real data from scenarios involving complicated remanence (i.e., many magnetized bodies with many magnetization directions). All tests provide favorable results and our methods compare well against those of other authors.

INTRODUCTION

The problem of remanence in magnetic interpretation

The total magnetization vector \vec{J}_{tot} within an isotropic body can be modeled as the vector sum

$$\vec{J}_{\text{tot}} = \chi \vec{H}_0 + \vec{J}_{\text{rem}}, \quad (1)$$

(Bossavit, 1998) where χ is magnetic susceptibility and \vec{H}_0 is the earth's magnetic field. The first term in equation 1 is the induced component of the magnetization,

$$\vec{J}_{\text{ind}} = \chi \vec{H}_0, \quad (2)$$

and \vec{J}_{rem} is the remanent component. Remanent magnetization (or remanence) is a permanent magnetization obtained in the past that often can be oriented in a direction different from the earth's field today. Hence, the induced and remanent components can be oriented in different directions.

Typical magnetic inversion routines such as that of Li and Oldenburg (1996) assume no remanent component exists. Hence, the magnetization is assumed to lie in the direction of the earth's field and erroneous results can be obtained if this assumption is made incorrectly. To demonstrate this, consider the following 3D synthetic example. Figure 1 depicts the model mesh with an overlaid schematic showing the magnetization of the central body: the earth's field has strength 40000 nT, is vertical and downward (an inclination of 90°), and the remanent magnetization is horizontal toward the east (right in this diagram, a declination of 90°). The Königsberger ratio

$$Q = \frac{|\vec{J}_{\text{rem}}|}{|\vec{J}_{\text{ind}}|} = \frac{|\vec{J}_{\text{rem}}|}{\chi |\vec{H}_0|} \quad (3)$$

for the body is set to unity ($Q = 1$) so that magnitudes of the induced and remanent magnetization components are equal; the resulting total magnetization is oriented with a 45° dip.

Figure 2 compares different contributions to the TMI (total magnetic intensity) response (TMI measurements are $B = \mu_0 H$). To invert this data, we use the methods of Li and Oldenburg (1996, 2003). Figure 3a shows the susceptibility model recovered from inversion of the data in Figure 2c assuming no remanence exists (i.e., assuming the total magnetization is in the direction of the earth's inducing field). The inversion had trouble converging (i.e., fitting the data)

Manuscript received by the Editor 10 October 2008; revised manuscript received 28 November 2008; published online 10 April 2009.
¹University of British Columbia, Department of Earth and Ocean Sciences, Geophysical Inversion Facility, Vancouver, British Columbia, Canada. E-mail: plelievre@eos.ubc.ca; doug@eos.ubc.ca.
© 2009 Society of Exploration Geophysicists. All rights reserved.

and the recovered model bears little resemblance to the true model, with significant susceptible material placed toward the mesh boundaries.

Previous approaches to dealing with remanence

Several authors have approached the problem of remanence by assuming simple causative bodies with uniform total magnetization directions. Li et al. (2004) provide an excellent summary of methods that can be used to estimate the total magnetization direction for such scenarios through analysis of the anomalies in magnetic data. The magnetization direction derived through these methods could be used in a subsequent inversion for an effective susceptibility χ_{eff} , equal to the magnetization amplitude divided by the earth's field strength:

$$\chi_{\text{eff}} = \frac{|\vec{J}_{\text{tot}}|}{|\vec{H}_0|} = \frac{|\chi\vec{H}_0 + \vec{J}_{\text{rem}}|}{|\vec{H}_0|}. \quad (4)$$

Methods include that of Phillips (2005), which makes use of Helbig's moment method (Helbig, 1963); the multiscale edge method of Haney and Li (2002), which makes use of a continuous wavelet transform; and the crosscorrelation method of Dannemiller and Li (2006), which uses the reduction-to-pole process. Those methods rely on an adequate separation between the anomalies from different bodies and assume that for each body a constant net magnetization direction is sufficient to describe the whole body. Generally, this simplistic scenario is not applicable to the mineral exploration applications of interest in this paper, where the subsurface magnetization

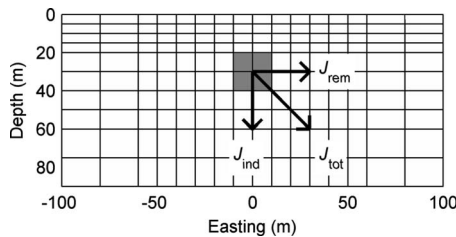


Figure 1. A vertical cross section at northing = 0 m through the true 3D synthetic model. The mesh cell spacing is identical in the easting and northing directions. A small magnetic body with $\chi = 0.1$ (plotted in gray here) resides in the center of the mesh within a nonmagnetic background. The induced component of the magnetization is labeled J_{ind} , the remanent component J_{rem} , and the total magnetization J_{tot} .

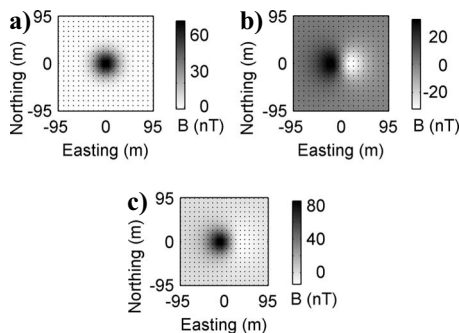


Figure 2. Map views of the (a) induced and (b) remanent components of the TMI response, and (c) total combined TMI response 10 m above the mesh in Figure 1.

can be complicated (e.g., varying remanence directions and amplitudes). Approaches discussed below are applicable to such complicated mineral exploration scenarios.

Another approach is to address properties of the measured magnetic field that are independent, or at least minimally dependent, on the direction of total magnetization. This removes the need to specify the direction of total magnetization exactly. Shearer and Li (2004) develop an algorithm that directly inverts a data quantity having a minimal dependence on the direction of the magnetization: they consider total gradient data (the amplitude of the anomalous magnetic field gradient). For 2D magnetics problems, this data quantity is independent of the magnetization direction, but it is weakly dependent in three dimensions. The algorithm of Shearer and Li (2004) incorporates fully the nonlinear relationship between the data and the subsurface magnetization. They invert for the magnitude of the magnetization on a 3D mesh without knowing the direction of magnetization. The advantage of their approach is that it is applicable to situations with complicated magnetic bodies and multiple remanence directions. Their forward computation requires prescription

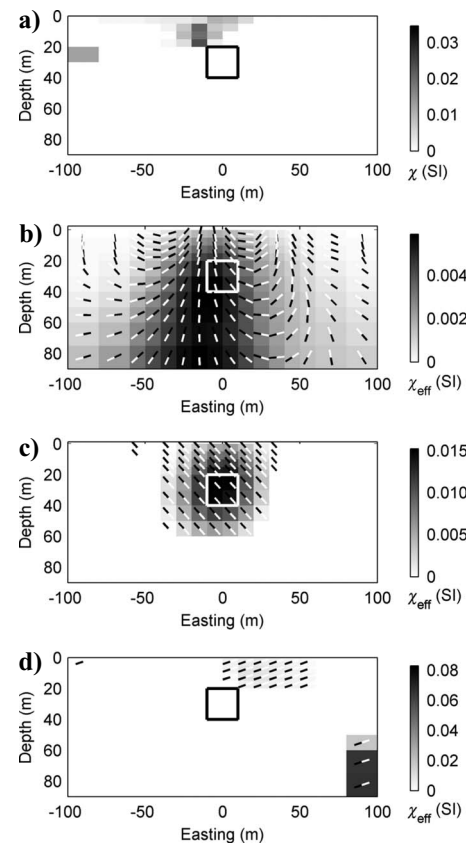


Figure 3. Vertical cross sections at northing = 0 m through 3D models recovered from inversion of the data in Figure 2c: (a) susceptibility inversion with positivity imposed and assuming no remanence exists; (b) TMVC inversion with $\gamma = 1$ and no bounding applied; (c) TMVS inversion with $\theta = 90^\circ$ in the initial half-space model; (d) TMVS inversion with $\theta = -45^\circ$ in the initial half-space model. The color scale used in (a) is SI susceptibility (unitless); in all others, it is magnetization amplitude in units of effective susceptibility (i.e., normalized by the earth's field strength). Total magnetization vectors are indicated by black and white lines with white at the head. Vectors with zero amplitude are not displayed. The black or white squares indicate the position of the block in the true model.

of some constant magnetization direction across the volume; in general, the prescribed direction will not correspond to the true direction. This can introduce some error into their inverse solutions and unacceptable artifacts (that would produce erroneous interpretations) can be recovered. Furthermore, if the total gradient data are not measured directly but is created instead from total field data through linear transforms, then further significant error can be introduced.

Whereas Shearer and Li (2004) invert for magnetization amplitude, our intention here is to calculate the magnetization amplitude and direction of the source distribution explicitly. The method of Shearer and Li (2004) deals with data that have a low sensitivity to one of the important quantities driving the magnetics problem: the magnetization direction. To recover the magnetization direction, it would be more appropriate to use data that are as sensitive to (i.e., contain enough information about) the magnetization as possible. Foss (2006) and Schmidt and Clark (2006) discuss how, compared to total magnetic intensity (TMI) data, three-component and gradient tensor magnetic data potentially can provide increased sensitivity to source magnetization direction. We go no further into those types of data here but mention that use of such data with our inversion methods that follow would be a fairly straightforward task.

INVERSION FOR MAGNETIZATION

To deal with the magnetic remanence problem, we invert magnetic data for a three-component subsurface magnetization vector, as opposed to magnetic susceptibility (a scalar). We consider two approaches: a Cartesian and a spherical framework, discussed below. For abbreviation purposes, we will refer to these methods as TMV (total magnetization vector) inversions, with TMVC denoting the Cartesian formulation and TMVS denoting the spherical formulation.

Wang et al. (2004) develop what they call a magnetization vector tomography imaging method. They recover a three-component Cartesian magnetization model but their approach is more applicable to determining the total magnetization direction of separated, homogeneous bodies. As previously stated, we are interested in more complicated scenarios. Parker et al. (1987) attempt to construct a three-component magnetization model that is the closest to a uniform solution (i.e., uniform magnetization direction). They use seminorm minimization and allow for an upper bound on the magnetization amplitude. We are interested in methods with more widespread applicability (i.e., allowing for more complicated causative magnetization).

Discretization of the TMV formulations

To invert for magnetization, we follow the methodology of Li and Oldenburg (1996) for inversion for isotropic susceptibility. In the susceptibility inversion, the model region is split into an orthogonal 3D mesh of M rectangular prismatic cells, each with constant susceptibility. If one assumes no remanence, the magnetization in the j th cell is in the direction of the earth's field and is

$$\vec{J}_j = \chi_j \vec{H}_0. \quad (5)$$

The N data predicted by the model (i.e., the response of the model), $\mathbf{d}^{\text{pred}} = [d_1, \dots, d_N]^T$, are calculated as

$$\mathbf{d}^{\text{pred}} = \mathbf{G}\boldsymbol{\chi}, \quad (6)$$

where $\boldsymbol{\chi} = [\chi_1, \dots, \chi_M]^T$ is the model vector containing the susceptibilities in each cell and \mathbf{G} is the N -by- M full sensitivity matrix.

The Cartesian formulation

In the TMVC formulation, the magnetization is split into one component parallel to the earth's field, and two components perpendicular to the earth's field. We define three orthogonal directions \hat{p} , \hat{s} , and \hat{t} with \hat{p} in the direction of the earth's field; \hat{s} and \hat{t} can be chosen in any convenient manner. The earth model vector \mathbf{m} contains the three components of magnetization in each cell:

$$\mathbf{m} = [\mathbf{p}, \mathbf{s}, \mathbf{t}]^T, \quad (7)$$

where $\mathbf{p} = [p_1, \dots, p_M]^T$ (similarly for \mathbf{s} and \mathbf{t}), and \mathbf{m} has length $3M$. We deal with units of effective susceptibility instead of magnetization strength by dividing the three magnetization components by the amplitude of the earth's field, H_0 . Then the magnetization in the j th cell is then written

$$\vec{J}_j = H_0(p_j\hat{p} + s_j\hat{s} + t_j\hat{t}), \quad (8)$$

and the predicted data are calculated as

$$\mathbf{d}^{\text{pred}} = \mathbf{G}_p\mathbf{p} + \mathbf{G}_s\mathbf{s} + \mathbf{G}_t\mathbf{t}. \quad (9)$$

The sensitivity matrices in equation 9 are related to that in equation 6. We simplify equation 9 as

$$\mathbf{d}^{\text{pred}} = \mathbf{G}_{pst}\mathbf{m}, \quad (10)$$

by defining

$$\mathbf{G}_{pst} = [\mathbf{G}_p, \mathbf{G}_s, \mathbf{G}_t]. \quad (11)$$

The spherical formulation

In the TMVS formulation, the magnetization is represented by an amplitude, denoted a , a dip angle θ (positive down), and an azimuthal angle ϕ (positive east of north). Now the model vector contains the amplitude and two angles in each cell:

$$\mathbf{m} = [\mathbf{a}, \theta, \phi]^T. \quad (12)$$

Again, we deal with the amplitude as an effective susceptibility (magnetization amplitude divided by earth's field strength H_0). We define Cartesian axes with $+x$ northing, $+y$ easting, and $+z$ down and let

$$\begin{aligned} \vec{u} &= \vec{J}_x, \\ \vec{v} &= \vec{J}_y, \\ \vec{w} &= \vec{J}_z. \end{aligned} \quad (13)$$

Cartesian magnetization components in the j th cell are determined through the following trigonometric expressions:

$$\begin{aligned} u_j &= a_j \cos(\theta_j) \cos(\phi_j), \\ v_j &= a_j \cos(\theta_j) \sin(\phi_j), \\ w_j &= a_j \sin(\theta_j). \end{aligned} \quad (14)$$

Predicted data are calculated as

$$\mathbf{d}^{\text{pred}} = \mathbf{G}_u \mathbf{u} + \mathbf{G}_v \mathbf{v} + \mathbf{G}_w \mathbf{w}. \quad (15)$$

Again, the sensitivity matrices in equation 15 are related to that of equation 6 and we simplify equation 15 as

$$\mathbf{d}^{\text{pred}} = \mathbf{G}_{uvw} \mathbf{k} \quad (16)$$

by defining

$$\mathbf{k} = [\mathbf{u}, \mathbf{v}, \mathbf{w}]^T \quad (17)$$

and

$$\mathbf{G}_{uvw} = [\mathbf{G}_u, \mathbf{G}_v, \mathbf{G}_w]. \quad (18)$$

An underdetermined optimization approach

Following Li and Oldenburg (1996), we formulate the inversion as an underdetermined problem with Tikhonov regularization. The objective function to be minimized is

$$\psi = \frac{1}{2} \psi_d + \frac{\beta}{2} \psi_m, \quad (19)$$

where ψ_d is the data misfit and ψ_m is a parameterized model objective function that provides flexibility to generate models with different characteristics. The regularization parameter β allows us to control the data fit.

The data misfit is

$$\psi_d = \|\mathbf{W}_d(\mathbf{d}^{\text{pred}} - \mathbf{d}^{\text{obs}})\|^2, \quad (20)$$

where \mathbf{d}^{obs} is the observed data and the weighting matrix \mathbf{W}_d contains measurement uncertainties as in Li and Oldenburg (1996). If the statistics of the noise on the data is Gaussian then the data misfit in equation 20 is a chi-squared variable with expected value equal to the number of data. Therefore in our synthetic inversions, we search for a value of β such that the misfit equals the number of data.

The Cartesian formulation

To simplify the mathematics, we absorb \mathbf{W}_d into the observed data and sensitivity matrices in equation 9 such that

$$\psi_d = \|\tilde{\mathbf{G}}_{pst} \mathbf{m} - \tilde{\mathbf{d}}^{\text{obs}}\|^2. \quad (21)$$

Our model objective function is

$$\begin{aligned} \psi_m = & \|\mathbf{W}_p(\mathbf{p} - \mathbf{p}_{\text{ref}})\|^2 + \gamma \|\mathbf{W}_s(\mathbf{s} - \mathbf{s}_{\text{ref}})\|^2 \\ & + \gamma \|\mathbf{W}_t(\mathbf{t} - \mathbf{t}_{\text{ref}})\|^2. \end{aligned} \quad (22)$$

The regularization functionals \mathbf{W}_p , \mathbf{W}_s , and \mathbf{W}_t in equation 22 are equivalent to \mathbf{W}_m in Li and Oldenburg (1996). They include the desire for model smoothness and the depth weighting required for the magnetics problem. Each term in equation 22 contains three smoothness terms, each of which involves a finite-difference operator for a different Cartesian direction. Reference models \mathbf{p}_{ref} , \mathbf{s}_{ref} , and \mathbf{t}_{ref} can be included if desired. Factor $\gamma \in (0, \infty)$ controls the amount of magnetization that is tolerated in a direction away from the earth's field: high values of γ will result in magnetization parallel to the earth's field and low values of γ will result in magnetization perpendicular to the earth's field.

To solve the inverse problem, we set the gradient of the objective function to zero and obtain an equation of the form $\mathbf{A}\mathbf{m} = \mathbf{b}$ to solve for the magnetization model \mathbf{m} :

$$\mathbf{A} = \tilde{\mathbf{G}}_{pst}^T \tilde{\mathbf{G}}_{pst} + \beta \begin{bmatrix} \mathbf{W}_p^T \mathbf{W}_p & 0 & 0 \\ 0 & \gamma \mathbf{W}_s^T \mathbf{W}_s & 0 \\ 0 & 0 & \gamma \mathbf{W}_t^T \mathbf{W}_t \end{bmatrix} \quad (23)$$

and

$$\mathbf{b} = \tilde{\mathbf{G}}_{pst}^T \tilde{\mathbf{d}}^{\text{obs}} + \beta \begin{bmatrix} \mathbf{W}_p^T \mathbf{W}_p \mathbf{p}_{\text{ref}} \\ \gamma \mathbf{W}_s^T \mathbf{W}_s \mathbf{s}_{\text{ref}} \\ \gamma \mathbf{W}_t^T \mathbf{W}_t \mathbf{t}_{\text{ref}} \end{bmatrix}. \quad (24)$$

The spherical formulation

Again, we absorb \mathbf{W}_d into the observed data and sensitivity matrices in equation 15 such that

$$\psi_d = \|\tilde{\mathbf{G}}_{uvw} \mathbf{k} - \tilde{\mathbf{d}}^{\text{obs}}\|^2. \quad (25)$$

Our model objective function is

$$\begin{aligned} \psi_m = & \|\mathbf{W}_a(\mathbf{a} - \mathbf{a}_{\text{ref}})\|^2 + \gamma \|\mathbf{W}_\theta(\boldsymbol{\theta} - \boldsymbol{\theta}_{\text{ref}})\|^2 \\ & + \gamma \|\mathbf{W}_\phi(\boldsymbol{\phi} - \boldsymbol{\phi}_{\text{ref}})\|^2. \end{aligned} \quad (26)$$

Again, the regularization functionals in equation 26 are equivalent to \mathbf{W}_m in Li and Oldenburg (1996), with each term in equation 26 containing three smoothness terms, each of which involving a finite difference operator for a different Cartesian direction. We keep the parameter γ in the TMVS formulation to allow us to deal with scaling issues; the amplitude values will generally lie across a different range than the angles and we can balance the terms in equation 26 by altering γ .

The forward modeling procedure in equation 25 is now a nonlinear operation because of the trigonometric conversion required in equation 14. We use an iterative Gauss-Newton approach to solve the resulting nonlinear inverse problem: we solve an equation of the form

$$\mathbf{H} \delta \mathbf{m} = -\mathbf{g}, \quad (27)$$

with \mathbf{g} the gradient (first model derivative of the objective function ψ), \mathbf{H} the Hessian (second model derivative), and $\delta \mathbf{m}$ a model perturbation. After solving for $\delta \mathbf{m}$, a line search is performed for an appropriate step length α (the expected value is close to one) and the model is updated as

$$\mathbf{m}^{(k+1)} = \mathbf{m}^{(k)} + \alpha \delta \mathbf{m}, \quad (28)$$

where $\mathbf{m}^{(k)}$ is the current iterate and $\mathbf{m}^{(k+1)}$ the updated model. The gradient \mathbf{g}_m and Hessian \mathbf{H}_m of the model objective function ψ_m are

$$\mathbf{g}_m = \begin{bmatrix} \mathbf{W}_a^T \mathbf{W}_a (\mathbf{a} - \mathbf{a}_{\text{ref}}) \\ \gamma \mathbf{W}_\theta^T \mathbf{W}_\theta (\boldsymbol{\theta} - \boldsymbol{\theta}_{\text{ref}}) \\ \gamma \mathbf{W}_\phi^T \mathbf{W}_\phi (\boldsymbol{\phi} - \boldsymbol{\phi}_{\text{ref}}) \end{bmatrix} \quad (29)$$

and

$$\mathbf{H}_m = \begin{bmatrix} \mathbf{W}_a^T \mathbf{W}_a & 0 & 0 \\ 0 & \gamma \mathbf{W}_\theta^T \mathbf{W}_\theta & 0 \\ 0 & 0 & \gamma \mathbf{W}_\phi^T \mathbf{W}_\phi \end{bmatrix}. \quad (30)$$

For the data misfit term ψ_d , we use the chain and product rules for matrix-vector equations. The chain rule gives

$$\frac{d\psi_d}{d\mathbf{m}} = \frac{\partial \psi_d}{\partial \mathbf{k}} \frac{d\mathbf{k}}{d\mathbf{m}} \quad (31)$$

and gradient \mathbf{g}_d of the misfit term is then

$$\mathbf{g}_d = \mathbf{S}^T \tilde{\mathbf{G}}_{uvw}^T \delta \mathbf{d}, \quad (32)$$

where

$$\mathbf{S} = \frac{d\mathbf{k}}{d\mathbf{m}} = \begin{bmatrix} \mathbf{S}_{ua} & \mathbf{S}_{u\theta} & \mathbf{S}_{u\phi} \\ \mathbf{S}_{va} & \mathbf{S}_{v\theta} & \mathbf{S}_{v\phi} \\ \mathbf{S}_{wa} & \mathbf{S}_{w\theta} & \mathbf{S}_{w\phi} \end{bmatrix} \quad (33)$$

and

$$\mathbf{S}_{ua} = \mathbf{S}_{ua}^T = \text{diag}(\mathbf{s}_{ua}) = \frac{d\mathbf{u}}{da}, \quad (34)$$

with similar definitions to equation 34 for any missing quantities. The diag function takes a length n vector and places it along the main diagonal of an $n \times n$ matrix. Let f be some $m \times m$ matrix (or vector) and g be $p \times q$, both being functions of some quantity x . The product rule for matrix-vector equations is then

$$\frac{df(x)g(x)}{dx} = (g^T \otimes \mathbf{I}_m) \frac{df}{dx} + (\mathbf{I}_q \otimes f) \frac{dg}{dx} \quad (35)$$

where \otimes is the Kronecker product and \mathbf{I}_m is an $m \times m$ identity matrix. The Hessian \mathbf{H}_d of the misfit term is then

$$\begin{aligned} \mathbf{H}_d &= \frac{d}{d\mathbf{m}} (\mathbf{S}^T \tilde{\mathbf{G}}_{uvw}^T \delta \mathbf{d}) \\ &= [(\delta \mathbf{d}^T \tilde{\mathbf{G}}_{uvw}) \otimes \mathbf{I}_m] \frac{d\mathbf{S}^T}{d\mathbf{m}} + \mathbf{S}^T \tilde{\mathbf{G}}_{uvw}^T \frac{d\delta \mathbf{d}}{d\mathbf{m}}, \end{aligned} \quad (36)$$

which, after some nontrivial algebra, works out to

$$\mathbf{H}_d = \mathbf{T}_u \mathbf{D}_u + \mathbf{T}_v \mathbf{D}_v + \mathbf{T}_w \mathbf{D}_w + \mathbf{S}^T \tilde{\mathbf{G}}_{uvw}^T \tilde{\mathbf{G}}_{uvw} \mathbf{S}, \quad (37)$$

where

$$\mathbf{T}_u = \begin{bmatrix} \mathbf{T}_{u,aa} & \mathbf{T}_{u,a\theta} & \mathbf{T}_{u,a\phi} \\ \mathbf{T}_{u,\theta a} & \mathbf{T}_{u,\theta\theta} & \mathbf{T}_{u,\theta\phi} \\ \mathbf{T}_{u,\phi a} & \mathbf{T}_{u,\phi\theta} & \mathbf{T}_{u,\phi\phi} \end{bmatrix}, \quad (38)$$

$$\mathbf{T}_{u,a\theta} = \text{diag}(\mathbf{t}_{u,a\theta}) = \frac{ds_{ua}}{d\theta}, \quad (39)$$

$$\mathbf{D}_u = \text{diag}([\tilde{\mathbf{G}}_u^T \delta \mathbf{d}, \tilde{\mathbf{G}}_u^T \delta \mathbf{d}, \tilde{\mathbf{G}}_u^T \delta \mathbf{d}]^T), \quad (40)$$

and

$$\delta \mathbf{d} = \tilde{\mathbf{G}}_{uvw} \mathbf{k} - \tilde{\mathbf{d}}^{\text{obs}}, \quad (41)$$

with similar definitions for any missing quantities. We do not include the derivation of the expressions in equations 32 and 37 because they are quite involved. The individual elements of the \mathbf{S} and \mathbf{T} quantities are simply first and second derivatives of the expressions in equation 14 with respect to a , θ , and ϕ . Note that we are performing full Newton steps here. A Gauss-Newton approach would neglect the three $\mathbf{T}_u \mathbf{D}_u$ terms in equation 37, but investigation has shown that those terms give an important contribution to the Hessian and cannot be neglected.

Inversion functionality and important practical considerations

The susceptibility inversion of Li and Oldenburg (1996, 2003) contains a high degree of nonuniqueness. To deal with this, Li and Oldenburg (2003) add depth weighting and allow for further geologic information to be incorporated through weighting functions and physical property bounds, the latter enabling a positivity constraint on the susceptibility to maintain physical reality. In our magnetization inversions, there are now three times as many model parameters and it is likely that additional information is required to obtain acceptable solutions. Therefore, we provide the same weighting and bounding functionality.

In the TMVC (Cartesian) formulation, we can define a lower bound p_L that determines the value above which the p component of the magnetization must lie. If one is sure that no remanence exists, then γ can be set to some high value and p_L set to zero such that all the recovered magnetizations must be in the direction of (i.e., parallel to) the earth's field. In the limit $\gamma \rightarrow \infty$, such an inversion is identical to a susceptibility inversion assuming no remanence. If some remanence is expected, one can allow increasing amounts by decreasing γ toward zero and p_L below zero. With no a priori information about remanence, γ should be set to unity and the p component not bounded.

An appropriate value for γ in the TMVS (spherical) formulation is difficult to estimate for any particular application. Hence, we suggest running several inversions with different values of γ . When γ is below a certain threshold, the smoothness regularization on the angle terms is essentially removed and the results exhibit very scattered magnetization directions. Above a certain threshold, the smoothness regularization on the angle terms becomes the primary focus and all magnetizations are in the same direction.

In the TMVS (spherical) formulation, depth weighting is applied only to the amplitude term in the model objective function. Care must be taken to only include smallness regularization on the angles when reference models are provided. The TMVS objective function is nonlinear, resulting from the trigonometric identities required in the forward modeling. Hence, there is a chance that the objective function in the spherical formulation will suffer from negative curvatures and multiple minima. Therefore, our inversion algorithm contains checks for negative curvature, ensuring that all step directions $\delta \mathbf{m}$ are descent directions. If $\delta \mathbf{m}$ is not a descent direction, we multiply $\delta \mathbf{m}$ by -1 and perform a more careful line search in equation 28 (because now the expected value of $\alpha = 1$ is no longer appropriate). The following section demonstrates the existence of multiple minima in a simple example. Methods for ameliorating this problem also are mentioned below.

A simple synthetic test

In mineral exploration applications, remanence can be significant and subsurface magnetization complicated; there might be different earth regions containing quite different remanence. In this section and sections that follow, we investigate some illustrative synthetic problems to improve understanding of our TMV inversion methods prior to applying them to real data. Here, the data in Figure 2c are inverted after adding a small amount of random noise (taken from normal distributions with zero mean and standard deviations equal to 2% of the absolute data values plus 1 nT).

Results for the Cartesian formulation

Without any prior assumptions on the direction of remanence, it is most appropriate to set $\gamma = 1$ and not enforce bounds on the magnetization (here, resulting in the model in Figure 3b). From a target-picking perspective, there is a dramatic improvement compared to the susceptibility inversion results (compare to Figure 3a).

Performing a TMVC inversion with no positivity on the p component is similar to performing a susceptibility inversion with no positivity (identical in the limit $\gamma \rightarrow \infty$). Our TMVC results mirror the well-known effect often seen in susceptibility inversions: magnetic material is pushed deeper when no positivity is enforced. Hence, we suggest reducing the power of the depth weighting when performing TMVC inversions.

Results for the spherical formulation

Results for the spherical formulation inversion are shown in Figure 3c and d. For the inversion in Figure 3c, the initial model was a half-space with $a = 0.001$, $\theta = 90^\circ$, and $\phi = 90^\circ$; i.e., the initial model specified a magnetization orientation in the direction of the earth's field (which is not the true direction of the magnetization), and no reference models were used. We set $\gamma = 1$ so that the terms θ and ϕ dominated the model objective function, resulting in a constant magnetization direction. The recovered model in Figure 3c shows further improvement on the Cartesian formulation results.

For the inversion in Figure 3d, the initial half-space model was altered to have $\theta = -45^\circ$. The inversion had trouble converging (the model does not fit the data to the desired degree) and the result indicates the existence of multiple minima in the TMVS formulation. For this synthetic example, the results recovered with the TMVS formulation essentially were identical to that in Figure 3c for any initial orientations within 90° of the true magnetization.

REDUCING THE NONUNIQUENESS IN TMV INVERSIONS

Inverting for a vector magnetization model rather than scalar susceptibility increases the nonuniqueness of the problem greatly, but inclusion of a priori information can improve the results. Morris et al. (2007) provide a discussion of what types of remanence information realistically could be available for constraining a magnetic inversion. Below we discuss how that information could be incorporated into our TMV inversions.

Total magnetization known exactly

Obtaining thorough and reliable measurements of the remanence direction on oriented samples is not a common practice because of

expense and difficulty. Morris et al. (2007) discuss methods for overcoming the difficulties involved. If oriented rock samples are available, then χ (susceptibility), Q (Königsberger ratio), and the remanence direction can be measured. These can be combined with knowledge of the earth's field to determine both the amplitude and direction of the total magnetization at the sample locations. This information can be incorporated easily into either of our TMV inversions through the reference models and associated weights or through bounds on the model parameters.

Measurements of χ and Q

Obtaining measurements of χ and Q from rock samples is a fairly common practice. Assume that sampled measurements of χ and Q are available but the direction of remanence is not. To incorporate this information into the TMVC (Cartesian) magnetization inversion, we start by writing the magnitudes of the induced, remanent, and total magnetization as

$$\begin{aligned} |\vec{J}_{\text{ind}}| &= \chi |\vec{H}_0| = \chi H_0, \\ |\vec{J}_{\text{rem}}| &= Q |\vec{J}_{\text{ind}}| = Q \chi H_0, \end{aligned} \quad (42)$$

and

$$|\vec{J}_{\text{tot}}| = |\vec{J}_{\text{ind}} + \vec{J}_{\text{rem}}|.$$

The maximum magnitude of the total magnetization occurs when the remanent and induced components are parallel, and the minimum occurs when those components are antiparallel (opposing). This reasoning provides the following inequality statements:

$$|1 - Q| \chi H_0 \leq |\vec{J}_{\text{tot}}| \leq (1 + Q) \chi H_0. \quad (43)$$

In the TMVC formulation, the total magnetization is

$$\vec{J}_{\text{tot}} = H_0(\vec{p} + \vec{s} + \vec{t}). \quad (44)$$

Hence, a constraint of the form

$$(1 - Q)^2 \chi^2 \leq p^2 + s^2 + t^2 \leq (1 + Q)^2 \chi^2 \quad (45)$$

can be included in the inverse problem. This is a fairly complicated nonlinear constraint and the minimization might be adversely affected. Much simpler bound constraints that follow similar reasoning are

$$\begin{aligned} (1 - Q)\chi &\leq p \leq (1 + Q)\chi, \\ -Q\chi &\leq s \leq Q\chi \end{aligned}$$

and

$$-Q\chi \leq t \leq Q\chi, \quad (46)$$

but these constraints provide more flexibility (are less constraining) than those in equation 45.

In contrast to the nonlinear constraints in equation 45, incorporating χ and Q information into the TMVS (spherical) magnetization inversion yields bounds on the magnetization amplitude:

$$|1 - Q| \chi \leq a \leq (1 + Q) \chi. \quad (47)$$

The method of Parker et al. (1987) also allows for an upper bound on the magnetization amplitude.

Known or assumed remanence direction

For most exploration boreholes, the core samples are only oriented well enough to determine the magnetic inclination θ , but not the declination ϕ . Morris et al. (2007) mention methods for approximating the declination using available geologic knowledge.

For the TMVC (Cartesian) formulation, if the direction of remanence can be assigned exactly, then a linear equality constraint of the form

$$\mathbf{s} + \mathbf{A}\mathbf{t} + \mathbf{b} = 0 \quad (48)$$

can be created, which results from the requirement that

$$s_j \hat{\mathbf{s}} + t_j \hat{\mathbf{t}} = \vec{J}_{\text{rem},\perp} \quad (49)$$

for all $j = 1 \dots M$ where $\vec{J}_{\text{rem},\perp}$ is the component of the remanence perpendicular to the earth's field. When the remanence direction can be only approximated, this information would result in inequality constraints related to the equality constraint in equation 48.

Sampled measurements of θ and/or ϕ can be incorporated into the TMVS (spherical) formulation through trivial use of the angle reference models or bounds. The direction of total magnetization lies somewhere between the remanence direction and the earth's field, leading to bounds on θ and ϕ in the TMVS formulation.

Comparison of constraints in the Cartesian and spherical formulations

It is clear from the above discussion that available geologic information can be incorporated into the spherical formulation much more easily than the Cartesian formulation. Assume that some combination of the true susceptibility, Königsberger ratio, remanence direction, and total magnetization direction are known in the cells containing the true anomalous block in Figure 1. Calculating equations 45 and 46 for those cells shows that the recovered model in Figure 3b already satisfies those constraint equations. Hence, it is apparent that those constraints might not provide much utility in the TMV inversions and the full magnetization direction could be required.

A COMPLICATED SYNTHETIC SCENARIO

Now we move on to a more complicated 3D synthetic scenario that could not be approached with methods that assume a uniform magnetization direction. The mesh and model are shown in Figure 4. The earth's field is oriented toward the north, inclined 30° above the horizontal, as indicated in Figure 4b. The remanent magnetization is different for each of the two vertical tabular bodies, as indicated in Figure 4c: the body to the west has a horizontal remanence directed 30° W of north; the body to the east has a horizontal remanence directed 30° E of north. The susceptibility of the bodies is 0.1 SI (within a zero background) and the Königsberger ratio is set to 3.0 for both bodies. This results in an effective susceptibility χ_{eff} of 0.38 for each body.

Figure 5a shows the result of inverting the data in Figure 6c using the method of Shearer and Li (2004). Figure 6 compares the different contributions to the TMI magnetic response of the true model in Figure 4. The method of Shearer and Li (2004) recovers an acceptable central body but there is significant magnetic material placed toward the mesh boundaries. We do not show the result of inverting the data in Figure 6c for susceptibility assuming no remanence exists, but as

expected, that inversion was slow to converge (it could not fit the data to the desired degree) and the recovered model showed little resemblance to the true model.

As previously mentioned, we suggest reducing the power of the depth weighting when performing TMVC inversions. Figures 5b and 7a show the result of a TMVC inversion with $\gamma = 1$ and the depth weighting power reduced from 3.0 to 2.0. The TMVC result is comparable in shape to that using the method of Shearer and Li (2004). The TMVC inversion recovered lower values because overall it placed the magnetic material a few cells closer to the surface (a result of the altered depth weighting). Note that some padding cells have been removed in the figures in this section that show cross-section plots.

Now we perform a TMVS inversion using knowledge gained from the TMVC result to constrain the TMVS inversion so that it does not approach inappropriate local minima. First, the TMVC result allows us to reduce the size of the active mesh region (i.e., removing padding cells) to reduce the nonuniqueness of the problem.

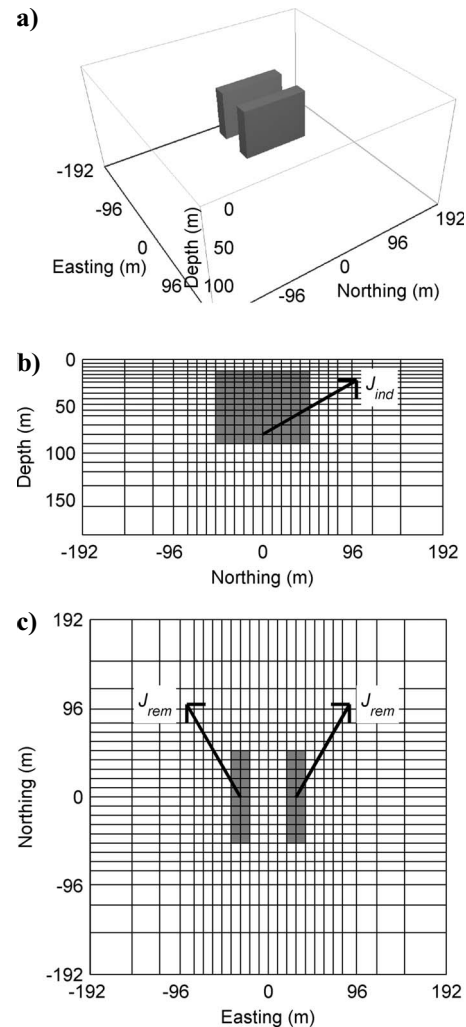


Figure 4. Views of the synthetic two body model: (a) shows a 3D perspective view, (b) shows a vertical cross section at easting = 30 m, and (c) shows a horizontal cross section at depth = 30 m. Mesh cell spacing is identical in the easting and northing directions. The induced component of the magnetization is indicated in (b) and the remanent component in (c).

Second, the TMVC result indicates a split in the azimuth of the magnetizations: the highest magnetizations to the west have negative azimuths, and those to the east have positive azimuths. This allows us to place bounds on ϕ in the TMVS inversion, with $\phi \in [-90, 0]$ in the west and $\phi \in [0, 90]$ in the east. This new TMVS inversion converged well. The result, seen in Figures 5c and 7b, shows drastic improvement over the TMVC result, now better indicating the presence of two vertical tabular bodies.

A REAL DATA EXAMPLE WITH MULTIPLE BODIES AND COMPLICATED REMANENCE

Here we invert real survey data over a region containing multiple bodies with complicated remanence. The data, shown in Figure 8, have been base-station corrected only. Therefore, we design the inversion mesh to have padding cells extending beyond the data region to allow for any regional component that might exist in the data. However, the magnetization inversions place little to no magnetic material in the padding cells, so we do not show those cells in the results. The region to the south contains several thin remanently magnetized units near the surface that have been tilted and faulted and,

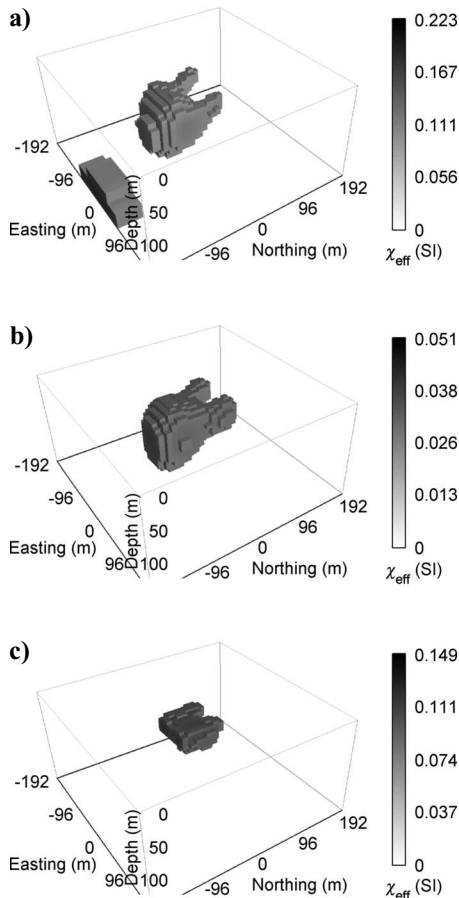


Figure 5. 3D perspective views of models recovered from inversion of the data in Figure 6c. Plot (a) shows a $\chi_{\text{eff}} = 0.10$ -SI isosurface of the model from a magnetization amplitude inversion (i.e., the method of Shearer and Li [2004]). Plot (b) shows a $\chi_{\text{eff}} = 0.032$ -SI isosurface of the model from a TMVC inversion with $\gamma = 1.0$ and a depth-weighting power of 2. Plot (c) shows a $\chi_{\text{eff}} = 0.11$ -SI isosurface of the model from a TMVS inversion with $\gamma = 1.0 \times 10^{-3}$ and bounds applied.

consequently, have remanent magnetizations oriented in many directions. This is evident in Figure 8 from the scattered small-scale anomalies near the south. A deeper intrusive body lies further to the north of the remanently magnetized surface units, represented by a longer-scale feature in the data.

We assign uncertainties to the data that are composed of 2% of the absolute data values plus a floor of 50 nT (which equals approximately 2% of the total data range). Unless otherwise mentioned, all inversions yield a chi-squared misfit value equal to the number of

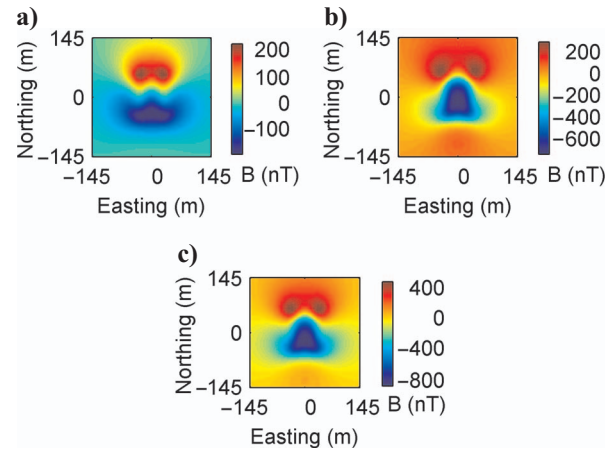


Figure 6. Map views of the (a) induced and (b) remanent components of the TMI response, and (c) total combined TMI response 10 m above the mesh in Figure 4.

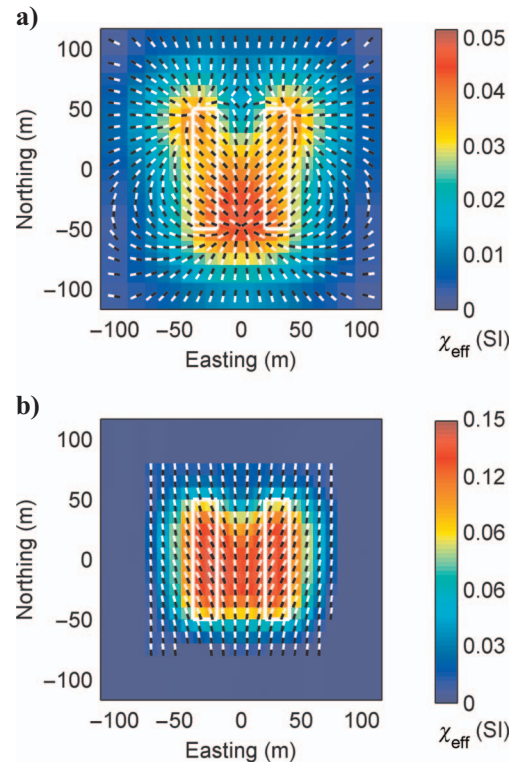


Figure 7. Plots (a) and (b) show horizontal cross sections at depth = 30 m through the models in Figures 5b and c, respectively. Total magnetization vectors are indicated by black and white lines with white at the head. Vectors with zero amplitude are not displayed. The white rectangles indicate the position of the blocks in the true model.

data ($= 7509$). We found that the magnetization inversions were able to fit the data easily and lead to results with a reasonable level of data fit and a reasonable amount of structure. This indicates that the assigned uncertainties were appropriate. However, inversions for susceptibility have trouble fitting the data and the recovered models have geologically unrealistic features and unrealistically high susceptibility values. Then the conclusion is that there is significant complicated remanence (high amplitude and many directions) in the subsurface that is affecting the susceptibility inversion results. In-

verting for susceptibility, and thereby assuming all magnetization in the region is parallel to the earth's field, is not appropriate in this case. We must move to a magnetization inversion.

For magnetization inversion, we use the Cartesian formulation (TMVC). We set $\gamma = 1.0$ to allow magnetization in any direction, and we weight the smallness term to balance the values of the smoothness and smallness terms for the recovered models. Figure 9 illustrates the result: Figure 9a shows the p component recovered and Figure 9b shows the amplitude of the remaining magnetization, which we denote the st component ($= \sqrt{s^2 + t^2}$). These results clearly indicate significant remanence near the surface toward the south (where the st component is high) and a large susceptible body with little to no remanence at depth toward the north (where the st component is low and the p component is high). This is consistent with knowledge of the geology.

CONCLUSIONS

Inverting magnetic data for all three vector components of the subsurface magnetization is one possible route to interpreting magnetic data complicated by remanence. We have developed two three-component magnetization inversion routines (in Cartesian and spherical frameworks) appropriate for use on data that contain the response of material exhibiting complicated magnetization (i.e., magnetization amplitude and direction varying throughout the region). The problem of remanence in magnetic inversions now can be dealt with through use of these two routines within an appropriate workflow, as indicated throughout this paper and discussed below.

Allowing a vector magnetization greatly increases the nonuniqueness of the magnetic inverse problem. We stress that the recovery of total magnetization is possible but it relies on incorporation of reliable geologic information regarding remanence. Specifically, point measurements of the magnetization magnitude and direction obtained from oriented drill core samples might be required to obtain acceptable magnetization models for more complicated scenarios. Therefore, we have designed our methods to allow incorporation of the types of information commonly collected.

The TMVC (Cartesian formulation) inversions tend to do a good job in the absence of additional information. In contrast, the TMVS (spherical formulation) inversions can perform poorly without an appropriate amount of constraints placed in them, but with those constraints TMVS inversions can outperform TMVC inversions. Information regarding remanence is more easily incorporated into the TMVS formulation. For these reasons, we suggest initial use of the TMVC formulation, followed by constrained TMVS inversions. With either routine, additional information incorporated as constraints can improve the results dramatically. However, because of the presence of multiple minima in the TMVS formulation, it is vital to set bounds based on the TMVC result so that the TMVS inversion does not approach inappropriate local minima.

In addition, it is important to note that our inversions recover the total magnetization, equal to the induced magnetization plus any existing remanence. The s and t components of the total magnetization are perpendicular to the inducing earth's field and are, therefore, associated only with the remanence. However, it is not possible to disentangle the induced magnetization and the component of the remanence in the same direction, both of which are combined in the p component of the total magnetization. The process of viscous remanent magnetization can cause a remanent component in the direction of the earth's field. Hence, the remanence is often aligned with the

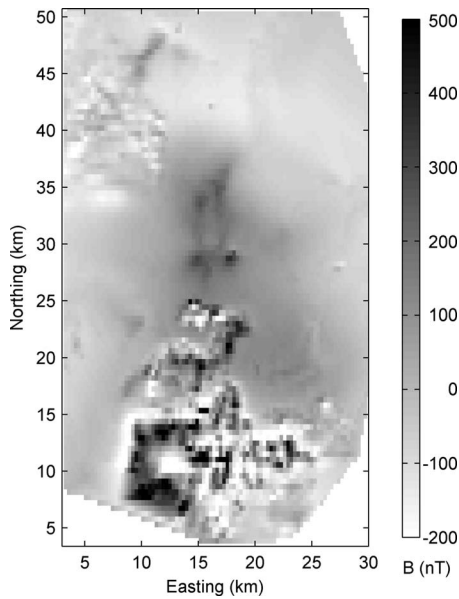


Figure 8. A map of the real TMI survey data. The data ranges from 726 nT to 1062 nT but we have altered the color scale here to better represent larger-scale data features.

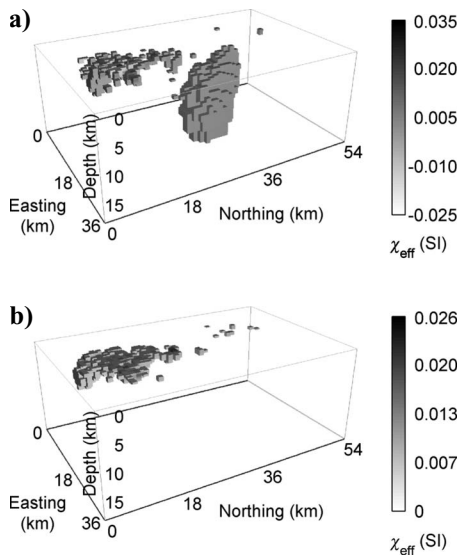


Figure 9. 3D perspective views from the southeast of the model recovered from a TMVC inversion of real survey data with $\gamma = 1.0$. Plot (a) shows $\chi_{\text{eff}} = -0.009$ -SI and $\chi_{\text{eff}} = +0.005$ -SI isosurfaces of the p component. Plot (b) shows a $\chi_{\text{eff}} = 0.006$ -SI isosurface of the st component model ($= \sqrt{s^2 + t^2}$).

current earth's field, in which case inversion methods assuming no remanence will behave well but return higher susceptibility values.

ACKNOWLEDGMENTS

We are grateful to Yaoguo Li for providing the inversion code associated with the method of Shearer and Li (2004); EDCON-PRJ for providing the real data; Ken Hickey for his help inverting the real data; and Nigel Phillips for his involvement in the preliminary testing of the TMVC methods. This manuscript was improved significantly by reviews from Olivier Boulanger, Mark Pilkington, and one anonymous reviewer.

REFERENCES

- Bossavit, A., 1998, Computational electromagnetism: Academic Press.
- Dannemiller, N., and Y. Li, 2006, A new method for determination of magnetization direction: *Geophysics*, **71**, no. 6, L69–L73.
- Foss, C., 2006, Improvements in source resolution that can be expected from inversion of magnetic field tensor data: *The Leading Edge*, **25**, 81–84.
- Haney, M., and Y. Li, 2002, Total magnetization direction and dip from multiscale edges: 72nd Annual International Meeting, SEG, Expanded Abstracts, 735–738.
- Helbig, K., 1963, Some integrals of magnetic anomalies and their relation to the parameters of the disturbing body: *Zeitschrift für Geophysik*, **29**, 83–96.
- Li, Y., and D. W. Oldenburg, 1996, 3D inversion of magnetic data: *Geophysics*, **61**, 394–408.
- , 2003, Fast inversion of large-scale magnetic data using wavelet transforms and logarithmic barrier method: *Geophysical Journal International*, **152**, 251–265.
- Li, Y., S. Shearer, M. Haney, and N. Dannemiller, 2004, Comprehensive approaches to the inversion of magnetic data with strong remanent magnetization: 74th Annual International Meeting, SEG, Expanded Abstracts, 1191–1194.
- Morris, B., H. Ugalde, and V. Thomson, 2007, Magnetic remanence constraints on magnetic inversion models: *The Leading Edge*, **26**, 960–964.
- Parker, R. L., L. Shure, and J. A. Hildebrand, 1987, The application of inverse theory to seamount magnetism: *Reviews of Geophysics*, **25**, 17–40.
- Phillips, J. D., 2005, Can we estimate total magnetization directions from aeromagnetic data using Helbig's integrals?: *Earth Planets Space*, **57**, 681–689.
- Schmidt, P. W., and D. A. Clark, 2006, The magnetic gradient tensor: its properties and uses in source characterization: *The Leading Edge*, **25**, 75–78.
- Shearer, S., and Y. Li, 2004, 3D inversion of magnetic total gradient data in the presence of remanent magnetization: 74th Annual International Meeting, SEG, Expanded Abstracts, 774–777.
- Wang, M., Q. Di, K. Xu, and R. Wang, 2004, Magnetization vector inversion equations and forward [*sic*] and inverse [*sic*] 2-d model study: *Chinese Journal of Geophysics*, **47**, 601–609.